Study of ψ(3686)→π^{0}h_{c}, h_{c}→γη_{c} via η_{c} exclusive decays

M. Ablikim *et al.* (BESIII Collaboration)

Phys. Rev. D **86**, 092009 — Published 19 November 2012

DOI: 10.1103/PhysRevD.86.092009

Study of $\psi(3686) \to \pi^0 h_c, h_c \to \gamma\eta_c$ via η_c exclusive decays

M. Ablikim[1], M. N. Achasov[5], O. Albayrak[3], D. J. Ambrose[39], F. F. An[1], Q. An[40], J. Z. Bai[1], Y. Ban[27], J. Becker[2], J. V. Bennett[17], M. Bertani[18A], J. M. Bian[38], E. Boger[20,a], O. Bondarenko[21], I. Boyko[20], R. A. Briere[3], V. Bytev[20], X. Cai[1], O. Cakir[35A], A. Calcaterra[18A], G. F. Cao[1], S. A. Cetin[35B], J. F. Chang[1], G. Chelkov[20,a], G. Chen[1], H. S. Chen[1], J. C. Chen[1], M. L. Chen[1], S. J. Chen[25], X. Chen[27], Y. B. Chen[1], H. P. Cheng[14], Y. P. Chu[1], D. Cronin-Hennessy[38], H. L. Dai[1], J. P. Dai[1], D. Dedovich[20], Z. Y. Deng[1], A. Denig[19], I. Denysenko[20,b], M. Destefanis[43A,43C], W. M. Ding[29], Y. Ding[23], L. Y. Dong[1], M. Y. Dong[1], S. X. Du[46], J. Fang[1], S. S. Fang[1], L. Fava[43B,43C], F. Feldbauer[2], C. Q. Feng[40], R. B. Ferroli[18A], C. D. Fu[1], J. L. Fu[25], Y. Gao[34], C. Geng[40], K. Goetzen[7], W. X. Gong[1], W. Gradl[19], M. Greco[43A,43C], M. H. Gu[1], Y. T. Gu[9], Y. H. Guan[6], A. Q. Guo[26], L. B. Guo[24], Y. P. Guo[26], Y. L. Han[1], F. A. Harris[37], K. L. He[1], M. He[1], Z. Y. He[26], T. Held[2], Y. K. Heng[1], Z. L. Hou[1], H. M. Hu[1], T. Hu[1], G. M. Huang[15], G. S. Huang[40], J. S. Huang[12], X. T. Huang[29], Y. P. Huang[1], T. Hussain[42], C. S. Ji[40], Q. Ji[1], Q. P. Ji[26,c], X. B. Ji[1], X. L. Ji[1], L. L. Jiang[1], X. S. Jiang[1], J. B. Jiao[29], Z. Jiao[14], D. P. Jin[1], S. Jin[1], F. F. Jing[34], N. Kalantar-Nayestanaki[21], M. Kavatsyuk[21], W. Kuehn[36], W. Lai[1], J. S. Lange[36], C. H. Li[1], Cheng Li[40], Cui Li[40], D. M. Li[46], F. Li[1], G. Li[1], H. B. Li[1], J. C. Li[1], K. Li[10], Lei Li[1], Q. J. Li[1], S. L. Li[1], W. D. Li[1], W. G. Li[1], X. L. Li[29], X. N. Li[1], X. Q. Li[26], X. R. Li[28], Z. B. Li[33], H. Liang[40], Y. F. Liang[31], Y. T. Liang[36], G. R. Liao[34], X. T. Liao[1], B. J. Liu[1], C. L. Liu[3], C. X. Liu[1], C. Y. Liu[1], F. H. Liu[30], Fang Liu[1], Feng Liu[15], H. Liu[1], H. H. Liu[13], H. M. Liu[1], H. W. Liu[1], J. P. Liu[44], K. Y. Liu[23], Kai Liu[6], P. L. Liu[29], Q. Liu[6], S. B. Liu[40], X. Liu[22], Y. B. Liu[26], Z. A. Liu[1], Zhiqiang Liu[1], Zhiqing Liu[1], H. Loehner[21], G. R. Lu[12], H. J. Lu[14], J. G. Lu[1], Q. W. Lu[30], X. R. Lu[6], Y. P. Lu[1], C. L. Luo[24], M. X. Luo[45], T. Luo[37], X. L. Luo[1], M. Lv[1], C. L. Ma[6], F. C. Ma[23], H. L. Ma[1], Q. M. Ma[1], S. Ma[1], T. Ma[1], X. Y. Ma[1], Y. Ma[11], F. E. Maas[11], M. Maggiora[43A,43C], Q. A. Malik[42], Y. J. Mao[27], Z. P. Mao[1], J. G. Messchendorp[21], J. Min[1], T. J. Min[1], R. E. Mitchell[17], X. H. Mo[1], C. Morales Morales[11], C. Motzko[2], N. Yu. Muchnoi[5], H. Muramatsu[39], Y. Nefedov[20], C. Nicholson[6], I. B. Nikolaev[5], Z. Ning[1], S. L. Olsen[28], Q. Ouyang[1], S. Pacetti[18B], J. W. Park[28], M. Pelizaeus[37], H. P. Peng[40], K. Peters[7], J. L. Ping[24], R. G. Ping[1], R. Poling[38], E. Prencipe[19], M. Qi[25], S. Qian[1], C. F. Qiao[6], X. S. Qin[1], Y. Qin[27], Z. H. Qin[1], J. F. Qiu[1], K. H. Rashid[42], G. Rong[1], X. D. Ruan[9], A. Sarantsev[20,d], B. D. Schaefer[17], J. Schulze[2], M. Shao[40],

C. P. Shen[37,e], X. Y. Shen[1], H. Y. Sheng[1], M. R. Shepherd[17], X. Y. Song[1], S. Spataro[43A,43C], B. Spruck[36], D. H. Sun[1], G. X. Sun[1], J. F. Sun[12], S. S. Sun[1], Y. J. Sun[40], Y. Z. Sun[1], Z. J. Sun[1], Z. T. Sun[40], C. J. Tang[31], X. Tang[1], I. Tapan[35C], E. H. Thorndike[39], D. Toth[38], M. Ullrich[36], G. S. Varner[37], B. Wang[9], B. Q. Wang[27], D. Wang[27], D. Y. Wang[27], K. Wang[1], L. L. Wang[1], L. S. Wang[1], M. Wang[29], P. Wang[1], P. L. Wang[1], Q. Wang[1], Q. J. Wang[1], S. G. Wang[27], X. L. Wang[40], Y. D. Wang[40], Y. F. Wang[1], Y. Q. Wang[29], Z. Wang[1], Z. G. Wang[1], Z. Y. Wang[1], D. H. Wei[8], J. B. Wei[27], P. Weidenkaff[19], Q. G. Wen[40], S. P. Wen[1], M. Werner[36], U. Wiedner[2], L. H. Wu[1], N. Wu[1], S. X. Wu[40], W. Wu[26], Z. Wu[1], L. G. Xia[34], Z. J. Xiao[24], Y. G. Xie[1], Q. L. Xiu[1], G. F. Xu[1], G. M. Xu[27], H. Xu[1], Q. J. Xu[10], X. P. Xu[32], Z. R. Xu[40], F. Xue[15], Z. Xue[1], L. Yan[40], W. B. Yan[40], Y. H. Yan[16], H. X. Yang[1], Y. Yang[15], Y. X. Yang[8], H. Ye[1], M. Ye[1], M. H. Ye[4], B. X. Yu[1], C. X. Yu[26], H. W. Yu[27], J. S. Yu[22], S. P. Yu[29], C. Z. Yuan[1], Y. Yuan[1], A. A. Zafar[42], A. Zallo[18A], Y. Zeng[16], B. X. Zhang[1], B. Y. Zhang[1], C. Zhang[25], C. C. Zhang[1], D. H. Zhang[1], H. H. Zhang[33], H. Y. Zhang[1], J. Q. Zhang[1], J. W. Zhang[1], J. Y. Zhang[1], J. Z. Zhang[1], S. H. Zhang[1], X. J. Zhang[1], X. Y. Zhang[29], Y. Zhang[1], Y. H. Zhang[1], Y. S. Zhang[9], Z. P. Zhang[40], Z. Y. Zhang[44], G. Zhao[1], H. S. Zhao[1], J. W. Zhao[1], K. X. Zhao[24], Lei Zhao[40], Ling Zhao[1], M. G. Zhao[26], Q. Zhao[1], Q. Z. Zhao[9,f], S. J. Zhao[46], T. C. Zhao[1], X. H. Zhao[25], Y. B. Zhao[1], Z. G. Zhao[40], A. Zhemchugov[20,a], B. Zheng[41], J. P. Zheng[1], Y. H. Zheng[6], B. Zhong[1], J. Zhong[2], Z. Zhong[9,f], L. Zhou[1], X. K. Zhou[6], X. R. Zhou[40], C. Zhu[1], K. Zhu[1], K. J. Zhu[1], S. H. Zhu[1], X. L. Zhu[34], Y. C. Zhu[40], Y. M. Zhu[26], Y. S. Zhu[1], Z. A. Zhu[1], J. Zhuang[1], B. S. Zou[1], J. H. Zou[1]

(BESIII Collaboration)

[1] *Institute of High Energy Physics, Beijing 100049, P. R. China*

[2] *Bochum Ruhr-University, 44780 Bochum, Germany*

[3] *Carnegie Mellon University, Pittsburgh, PA 15213, USA*

[4] *China Center of Advanced Science and Technology, Beijing 100190, P. R. China*

[5] *G.I. Budker Institute of Nuclear Physics SB RAS (BINP), Novosibirsk 630090, Russia*

[6] *Graduate University of Chinese Academy of Sciences, Beijing 100049, P. R. China*

[7] *GSI Helmholtzcentre for Heavy Ion Research GmbH, D-64291 Darmstadt, Germany*

[8] *Guangxi Normal University, Guilin 541004, P. R. China*

[9] *GuangXi University, Nanning 530004,P.R.China*

[10] *Hangzhou Normal University, Hangzhou 310036, P. R. China*

[11] *Helmholtz Institute Mainz, J.J. Becherweg 45,D 55099 Mainz,Germany*

[12] *Henan Normal University, Xinxiang 453007, P. R. China*

[13] *Henan University of Science and Technology, Luoyang 471003, P. R. China*

[14] *Huangshan College, Huangshan 245000, P. R. China*

[15] *Huazhong Normal University, Wuhan 430079, P. R. China*

[16] *Hunan University, Changsha 410082, P. R. China*

[17] *Indiana University, Bloomington, Indiana 47405, USA*

[18] *(A)INFN Laboratori Nazionali di Frascati, Frascati, Italy;*

(B)INFN and University of Perugia, I-06100, Perugia, Italy

[19] *Johannes Gutenberg University of Mainz,*

Johann-Joachim-Becher-Weg 45, 55099 Mainz, Germany

[20] *Joint Institute for Nuclear Research, 141980 Dubna, Russia*

[21] *KVI/University of Groningen, 9747 AA Groningen, The Netherlands*

[22] *Lanzhou University, Lanzhou 730000, P. R. China*

[23] *Liaoning University, Shenyang 110036, P. R. China*

[24] *Nanjing Normal University, Nanjing 210046, P. R. China*

[25] *Nanjing University, Nanjing 210093, P. R. China*

[26] *Nankai University, Tianjin 300071, P. R. China*

[27] *Peking University, Beijing 100871, P. R. China*

[28] *Seoul National University, Seoul, 151-747 Korea*

[29] *Shandong University, Jinan 250100, P. R. China*

[30] *Shanxi University, Taiyuan 030006, P. R. China*

[31] *Sichuan University, Chengdu 610064, P. R. China*

[32] *Soochow University, Suzhou 215006, China*

[33] *Sun Yat-Sen University, Guangzhou 510275, P. R. China*

[34] *Tsinghua University, Beijing 100084, P. R. China*

[35] *(A)Ankara University, Ankara, Turkey; (B)Dogus University,*

Istanbul, Turkey; (C)Uludag University, Bursa, Turkey

[36] *Universitaet Giessen, 35392 Giessen, Germany*

[37] *University of Hawaii, Honolulu, Hawaii 96822, USA*

[38] *University of Minnesota, Minneapolis, MN 55455, USA*

[39] *University of Rochester, Rochester, New York 14627, USA*

[40] *University of Science and Technology of China, Hefei 230026, P. R. China*

[41] *University of South China, Hengyang 421001, P. R. China*

[42] *University of the Punjab, Lahore-54590, Pakistan*

[43] *(A)University of Turin, Turin, Italy; (B)University of Eastern Piedmont, Alessandria, Italy; (C)INFN, Turin, Italy*

[44] *Wuhan University, Wuhan 430072, P. R. China*

[45] *Zhejiang University, Hangzhou 310027, P. R. China*

[46] *Zhengzhou University, Zhengzhou 450001, P. R. China*

[a] *also at the Moscow Institute of Physics and Technology, Moscow, Russia*

[b] *on leave from the Bogolyubov Institute for Theoretical Physics, Kiev, Ukraine*

[c] *Nankai University, Tianjin,300071,China*

[d] *also at the PNPI, Gatchina, Russia*

[e] *now at Nagoya University, Nagoya, Japan*

[f] *Guangxi University,Nanning,530004,China*

Abstract

The process $\psi(3686) \to \pi^0 h_c, h_c \to \gamma\eta_c$ has been studied with a data sample of 106 ± 4 million $\psi(3686)$ events collected with the BESIII detector at the BEPCII storage ring. The mass and width of the P-wave charmonium spin-singlet state $h_c(^1P_1)$ are determined by simultaneously fitting distributions of the π^0 recoil mass for 16 exclusive η_c decay modes. The results, $M(h_c) = 3525.31 \pm 0.11$ (stat.) ± 0.14 (syst.) MeV/c^2 and $\Gamma(h_c) = 0.70 \pm 0.28 \pm 0.22$ MeV, are consistent with and more precise than previous measurements. We also determine the branching ratios for the 16 exclusive η_c decay modes, five of which have not been measured previously. New measurements of the η_c line-shape parameters in the $E1$ transition $h_c \to \gamma\eta_c$ are made by selecting candidates in the h_c signal sample and simultaneously fitting the hadronic mass spectra for the 16 η_c decay channels. The resulting η_c mass and width values are $M(\eta_c) = 2984.49 \pm 1.16 \pm 0.52$ MeV/c^2 and $\Gamma(\eta_c) = 36.4 \pm 3.2 \pm 1.7$ MeV.

PACS numbers: 14.40.Pq, 13.25.Gv, 12.38.Qk

I. INTRODUCTION

Studies of charmonium states have played an important role in understanding Quantum Chromodynamics (QCD) because of their relative immunity from complications like relativistic effects and the large value of the strong coupling constant α_s. In the QCD potential model [1], the spin-independent one-gluon exchange part of the $c\bar{c}$ interaction has been defined quite well by existing experimental data. The spin dependence of the $c\bar{c}$ potential is not as well understood. Until recently, the only well-measured hyperfine splitting was that for the $1S$ states of charmonium, $\Delta M_{hf}(1S) = M(J/\psi) - M(\eta_c) = 116 \pm 1\,\mathrm{MeV}/c^2$ [2]. In the past several years Belle [3], CLEO [4], BaBar [5], and BESIII [6] have succeeded in identifying $\eta_c(2S)$ and have measured $\Delta M_{hf}(2S) = M(\psi(3686)) - M(\eta_c(2S)) = 47 \pm 1\,\mathrm{MeV}/c^2$.

Of the charmonium states below $D\bar{D}$ threshold, the $h_c(1^1P_1)$ is experimentally the least accessible because it cannot be produced directly in e^+e^- annihilation or in the electric-dipole transition of a $J^{PC} = 1^{--}$ charmonium state. Limited statistics and photon-detection challenges also were major obstacles to the observation of h_c in charmonium transitions. The precise measurement of h_c properties is important because a comparison of its mass with the masses of the $3P$ states (χ_{cJ}) provides much-needed information about the spin dependence of the $c\bar{c}$ interaction. According to QCD potential models, the $c\bar{c}$ interaction in a charmonium meson can be described with a potential that includes a Lorentz scalar confinement term and a vector Coulombic term arising from one-gluon exchange between the quark and the antiquark. The scalar confining potential makes no contribution to the hyperfine interaction and the Coulombic vector potential produces hyperfine splitting only for S states. This leads to the prediction of the hyperfine or triplet-singlet splitting in the P states of $M_{hf} \equiv \langle M(1^3P)\rangle - M(1^1P_1) \simeq 0$, where $\langle M(1^3P)\rangle$ is the spin-weighted centroid mass of the triplet ^3P_J states [7–9].

The first evidence of the h_c state was reported by the Fermilab E760 experiment [10] and was based on the process $p\bar{p} \to \pi^0 J/\psi$. This result was subsequently excluded by the successor experiment E835 [8], which investigated the same reaction with a larger data sample. E835 also studied $p\bar{p} \to h_c \to \gamma\eta_c$, in this case finding an h_c signal. Soon after this the CLEO collaboration observed the h_c and measured its mass [9, 11] by studying the decay chain $\psi(3686) \to \pi^0 h_c, h_c \to \gamma\eta_c$ in e^+e^- collisions. CLEO subsequently presented evidence for h_c decays to multi-pion final states [12]. Recently, the BESIII collaboration

used inclusive methods to make the first measurements of the absolute branching ratios $\mathcal{B}(\psi(3686) \to \pi^0 h_c) = (8.4 \pm 1.3 \pm 1.0) \times 10^{-4}$ and $\mathcal{B}(h_c \to \gamma\eta_c) = (54.3 \pm 6.7 \pm 5.2)\%$ [13]. CLEO has confirmed the BESIII results [14] and also observed h_c in $e^+e^- \to \pi^+\pi^- h_c$ at $\sqrt{s} = 4170\,\mathrm{MeV}$, demonstrating a new prolific source of h_c [15].

$\eta_c(1S)$ is the lowest-lying S-wave spin-singlet charmonium state. Although it has been known for about thirty years [16], its resonant parameters are still interesting. For a long time, measurements of the η_c width from B-factories and from charmonium transitions were inconsistent [2]. The discrepancies can be attributed to poor statistics and inadequate consideration of interference between η_c decays and non-resonant backgrounds. Besides, the η_c line shape also could be distorted by photon energy dependence in the $M1$ (or $E1$) transition, which will affect the resonant-parameter measurements. Recent studies by Belle, Babar, CLEO, and BESIII [17–20], with large data samples and careful consideration of interference, obtained similar η_c width and mass results in two-photon-fusion production and $\psi(3686)$ decays. The $h_c \to \gamma\eta_c$ transition can provide a new laboratory to study η_c properties. The η_c line shape in the $E1$ transition $h_c \to \gamma\eta_c$ should not be as distorted as in other charmonium decays, because non-resonant interfering backgrounds to the dominant transition are small.

In this paper, we report new measurements of the mass and width of the h_c and η_c, and of the branching ratios $\mathcal{B}_1(\psi(3686) \to \pi^0 h_c) \times \mathcal{B}_2(h_c \to \gamma\eta_c) \times \mathcal{B}_3(\eta_c \to X_i)$ and $\mathcal{B}_3(\eta_c \to X_i)$, via the sequential process $\psi(3686) \to \pi^0 h_c,\ h_c \to \gamma\eta_c,\ \eta_c \to X_i$. In this reaction X_i signifies 16 exclusive hadronic final states: $p\bar{p}$, $2(\pi^+\pi^-)$, $2(K^+K^-)$, $K^+K^-\pi^+\pi^-$, $p\bar{p}\pi^+\pi^-$, $3(\pi^+\pi^-)$, $K^+K^-2(\pi^+\pi^-)$, $K^+K^-\pi^0$, $p\bar{p}\pi^0$, $K^0_S K^\pm\pi^\mp$, $K^0_S K^\pm\pi^\mp\pi^\pm\pi^\mp$, $\pi^+\pi^-\eta$, $K^+K^-\eta$, $2(\pi^+\pi^-)\eta$, $\pi^+\pi^-\pi^0\pi^0$, and $2(\pi^+\pi^-)\pi^0\pi^0$. Here K^0_S is reconstructed in its $\pi^+\pi^-$ decays, and η in its $\gamma\gamma$ final state. The data sample of $\psi(3686)$ events was collected with the BESIII detector at the BEPCII e^+e^- storage ring.

The remainder of this paper is structured as follows: Sect. II describes the experiment and data sample; Sect. III presents the event selection and background analysis; Sect. IV discusses the extraction of h_c and η_c results; Sect. V describes the estimation of systematic uncertainties; and Sec. VI provides a summary and discussion of the results.

II. EXPERIMENT AND DATA SAMPLE

BEPCII is a two-ring e^+e^- collider designed for a peak luminosity of $10^{33}\,\mathrm{cm}^{-2}s^{-1}$ at a beam current of 0.93 A per beam. The cylindrical core of the BESIII detector consists of a helium-gas-based drift chamber (MDC) for charged-particle tracking and particle identification by $\mathrm{d}E/\mathrm{d}x$, a plastic scintillator time-of-flight system (TOF) for additional particle identification, and a 6240-crystal CsI(Tl) Electromagnetic Calorimeter (EMC) for electron identification and photon detection. These components are all enclosed in a superconducting solenoidal magnet providing a 1.0-T magnetic field. The solenoid is supported by an octagonal flux-return yoke with resistive-plate-counter muon detector modules (MUC) interleaved with steel. The geometrical acceptance for charged tracks and photons is 93% of 4π, and the resolutions for charged-track momentum and photon energy at 1 GeV are 0.5% and 2.5%, respectively. More details on the features and capabilities of BESIII are provided in Ref. [21].

The data sample for this analysis consists of $156.4\,\mathrm{pb}^{-1}$ of e^+e^- annihilation data collected at a center-of-mass energy of 3.686 GeV, the peak of the $\psi(3686)$ resonance. By measuring the production of multihadronic events we determine the number of $\psi(3686)$ decays in the sample to be $(1.06 \pm 0.04) \times 10^8$, where the uncertainty is dominated by systematics [22]. An additional $42\,\mathrm{pb}^{-1}$ of data were collected at a center-of-mass energy of 3.65 GeV to determine non-resonant continuum background contributions.

The optimization of the event selection and the estimation of physics backgrounds are performed with simulated Monte Carlo (MC) samples. A `GEANT4`-based [23, 24] detector simulation package is used to model the detector response. Signal and background processes are generated with specialized models that have been packaged and customized for BESIII [25]. The $\psi(3686)$ resonance is generated by `KKMC` [26], and `EvtGen` [27] is used to model events for $\psi(3686) \to \pi^0 h_c$ and for exclusive backgrounds in $\psi(3686)$ decays. An inclusive sample (100 million events) is used to simulate hadronic background processes. Known $\psi(3686)$ decay modes are generated with `EvtGen`, using branching ratios set to world-average values [2]. The remaining $\psi(3686)$ decay modes are generated by `LUNDCHARM` [25], which is based on `JETSET` [28] and tuned for the charm-energy region. The decays $\psi(3686) \to \pi^0 h_c$ are excluded from this sample.

The $\psi(3686) \to \pi^0 h_c$ events are generated with an h_c mass of $3525.28\,\mathrm{MeV}/c^2$ and a

width equal to that of the χ_{c1} (0.9 MeV). The $E1$ transition $h_c \to \gamma\eta_c$ is generated with an angular distribution in the h_c rest frame of $1 + \cos^2\theta^*$, where θ^* is the angle of the E1 photon with respect to the beam direction in the h_c rest frame. Multi-body η_c decays are generated according to phase space.

III. EVENT SELECTION AND BACKGROUND ANALYSIS

For $\psi(3686) \to \pi^0 h_c$, $h_c \to \gamma\eta_c$, the expected π^0 momentum is $P_{\pi^0} \simeq 84\,\mathrm{MeV}/c$, and the $E1$ transition photon emitted in $h_c \to \gamma\eta_c$ has an expected energy of $E(\gamma_{\rm E1}) \simeq 503\,\mathrm{MeV}$ in the h_c rest frame. Therefore, the signal candidates should have one $E1$ photon candidate with energy in the expected region $450\,\mathrm{MeV} < \mathrm{E}(\gamma_{\rm E1}) < 550\,\mathrm{MeV}$ and one π^0 candidate with recoil mass in the region $(3480, 3570)\,\mathrm{MeV/c^2}$. For the selected candidates, we fit the distribution of π^0 recoil mass for the full event sample to give the results for the h_c resonant parameters and signal yields.

Charged tracks in BESIII are reconstructed from MDC hits within a polar-angle (θ) acceptance range of $|\cos\theta| < 0.93$. To optimize the momentum measurement, we require that these tracks be reconstructed to pass within 10 cm of the interaction point in the beam direction and within 1 cm in the plane perpendicular to the beam. Tracks used in reconstructing K^0_S decays are exempted from these requirements.

A vertex fit constrains charged tracks to a common production vertex, which is updated on a run-by-run basis. For each charged track, time-of-flight and $\mathrm{d}E/\mathrm{d}x$ information is combined to compute particle identification (PID) confidence levels for the pion, kaon, and proton hypotheses. The track is assigned to the particle type with the highest confidence level.

Electromagnetic showers are reconstructed by clustering EMC crystal energies. Efficiency and energy resolution are improved by including energy deposits in nearby TOF counters. A photon candidate is defined as a shower with an energy deposit of at least 25 MeV in the "barrel" region ($|\cos\theta| < 0.8$), or of at least 50 MeV in the "end-cap" region ($0.86 < |\cos\theta| < 0.92$). Showers at angles intermediate between the barrel and the end-cap are not well measured and are rejected. An additional requirement on the EMC hit timing suppresses electronic noise and energy deposits unrelated to the event.

A candidate $\pi^0(\eta)$ is reconstructed from pairs of photons with an invariant mass in the

range $|M_{\gamma\gamma} - m_{\pi^0}| < 15\,\mathrm{MeV/c^2}$ ($|M_{\gamma\gamma} - m_{\eta}| < 15\,\mathrm{MeV/c^2}$) [2]. A one-constraint (1-C) kinematic fit is performed to improve the energy resolution, with the $M(\gamma\gamma)$ constrained to the known $\pi^0(\eta)$ mass.

We reconstruct $K^0_S \to \pi^+\pi^-$ candidates using pairs of oppositely charged tracks with an invariant mass in the range $|M_{\pi\pi} - m_{K^0_S}| < 20\,\mathrm{MeV/c^2}$, where $m_{K^0_S}$ is the known K^0_S mass [2]. To reject random $\pi^+\pi^-$ combinations, a secondary-vertex fitting algorithm is employed to impose the kinematic constraint between the production and decay vertices [29]. Accepted K^0_S candidates are required to have a decay length of at least twice the vertex resolution.

The η_c candidate is reconstructed in 16 exclusive decay modes, and the event is accepted or rejected based on consistency with the $h_c \to \gamma\eta_c$ hypothesis. Specifically, the reconstructed mass $M(\eta_c)$ is required to be between $2.900\,\mathrm{GeV}/c^2$ and $3.050\,\mathrm{GeV}/c^2$, and the transition-photon energy is required to be between 0.450 GeV and 0.550 GeV. Events passing this selection are subjected to a 4 constraint (4-C) kinematic fit to take advantage of energy-momentum conservation between the initial state (e^+e^- beams) and the final state (η_c + $E1$ photon + π^0). Because of differing signal/background characteristics, we individually optimize requirements on χ^2_{4C}, the χ^2 of the 4-C fit, for the 16 η_c channels. If multiple η_c candidates are found in an event, the one with the smallest value of $\chi^2 = \chi^2_{\rm 4C} + \chi^2_{\rm 1C} + \chi^2_{\rm pid} + \chi^2_{\rm vertex}$ is accepted, where $\chi^2_{\rm 1C}$ is the χ^2 of the 1-C fit of the $\pi^0(\eta)$, $\chi^2_{\rm pid}$ is the PID χ^2 summation for all charged tracks included in the h_c candidate, and $\chi^2_{\rm vertex}$ is the χ^2 of the K^0_S vertex fit. If there is no π^0/η (K^0_S) in an event, the corresponding $\chi^2_{\rm 1C}$ ($\chi^2_{\rm vertex}$) is set to zero.

Based on studies of the inclusive MC sample, we identified several background processes with potential to reduce the precision of measurements made with specific η_c exclusive channels because of sizable low-energy π^0 production. The processes and suppression procedures are as follows:

- $\psi(3686) \to \pi^+\pi^- J/\psi$

  The mass M_X of the system recoiling against the $\pi^+\pi^-$ in $\psi(3686) \to \pi^+\pi^- X$ is calculated and the candidate is rejected if M_X is within $\pm 12\,\mathrm{MeV}/c^2$ of the known J/ψ mass.

- $\psi(3686) \to \pi^0\pi^0 J/\psi$

The mass M_X of the system recoiling against the $\pi^0\pi^0$ in $\psi(3686) \to \pi^0\pi^0 X$ is calculated and the candidate is rejected if M_X is within $\pm 15\,\mathrm{MeV}/c^2$ of the known J/ψ mass for all η_c final states except $\pi^+\pi^-\pi^+\pi^-\pi^0\pi^0$. For this mode the lower π^0 momentum leads to recoil masses near $3.1\,\mathrm{GeV}/c^2$, so the exclusion window is narrowed to $\pm 10\,\mathrm{MeV}/c^2$.

- $\psi(3686) \to \gamma\chi_{c2}$

  A candidate is rejected if it includes a π^0 for which either daughter photon has an energy within $\pm 5\,\mathrm{MeV}$ of that expected for the $\psi(3686)$ radiative transition to χ_{c2} ($128\,\mathrm{MeV}$).

- *$E1$ photon candidates that are π^0 decay products*

  A candidate is rejected if its $E1$ photon can be combined with another photon in the event to form a π^0 within a mass window of $\pm 10\,\mathrm{MeV}/c^2$.

- *π^0 candidates that are from $\eta \to \pi^+\pi^-\pi^0$*

  Masses $M(\pi^+\pi^-\pi^0)$ are calculated for all possible combinations in the event and the candidate is rejected if any combination has a mass within $\pm 15\,\mathrm{MeV}/c^2$ of the known η mass.

Decisions about whether to apply a requirement to a particular η_c mode and the optimization of the χ^2_{4C} and PID requirements were made on a channel-by-channel basis. The figure-of-merit used was $\mathcal{S} = N_S/\sqrt{N_S + N_B}$, where N_S is the number of signal and N_B the number of background candidates. PDG values [2] are used for the input η_c branching ratios, and for channels not tabulated by the PDG we estimate branching ratios based on conjugate channels or other similar modes. The optimized selection criteria are listed in Table I, in which the $N(p)$, $N(\pi)$ and $N(K)$ denote the numbers of identified protons, pions and kaons in an event.

The π^0 recoil mass spectra for events passing these requirements show clear h_c signals in the expected range, as can be seen in Fig. 1. No peaking backgrounds in the signal region are found in the 100-million-event inclusive MC sample, in the continuum data sample taken at $\sqrt{s} = 3.65\,\mathrm{GeV}$, or in η_c-candidate-mass side-band distributions.

TABLE I: Event-selection requirements for each exclusive channel.

Mode	χ^2_{4C}	PID	$\pi^+\pi^- J/\psi$ veto	$\pi^0\pi^0 J/\psi$ veto	$\gamma\chi_{c2}$ veto	π^0 veto for $E1$ photon	$\eta \to \pi^+\pi^-\pi^0$ veto
$p\bar{p}$	30	$N(p) \geq 1$	no	no	yes	no	no
$\pi^+\pi^-\pi^+\pi^-$	60	$N(\pi) \geq 3$	yes	yes	yes	yes	yes
$K^+K^-K^+K^-$	60	$N(K) \geq 3$	no	no	no	yes	no
$K^+K^-\pi^+\pi^-$	40	$N(K) \geq 2, N(\pi) \geq 0$	yes	yes	yes	yes	yes
$p\bar{p}\pi^+\pi^-$	30	$N(p) \geq 2, N(\pi) \geq 0$	yes	yes	yes	yes	yes
$\pi^+\pi^-\pi^+\pi^-\pi^-\pi^-$	50	$N(\pi) \geq 4$	yes	yes	no	yes	yes
$K^+K^-\pi^+\pi^-\pi^-\pi^-$	70	$N(K) \geq 2, N(\pi) \geq 2$	yes	no	no	no	no
$K^+K^-\pi^0$	50	$N(K) \geq 1$	no	yes	no	no	no
$p\bar{p}\pi^0$	40	$N(p) \geq 1$	no	yes	yes	yes	no
$K^0_S K^\pm\pi^\mp$	70	–	no	no	no	no	yes
$K^0_S K^\pm\pi^\mp\pi^\pm\pi^\mp$	50	–	no	no	yes	no	no
$\pi^+\pi^-\eta$	50	–	no	no	no	yes	no
$K^+K^-\eta$	70	$N(K) \geq 1$	no	no	yes	yes	no
$\pi^+\pi^-\pi^+\pi^-\eta$	30	–	yes	no	no	yes	no
$\pi^+\pi^-\pi^0\pi^0$	40	–	yes	yes	yes	yes	yes
$\pi^+\pi^-\pi^+\pi^-\pi^0\pi^0$	60	–	yes	yes	no	yes	no

IV. EXTRACTION OF YIELDS AND RESONANCE PARAMETERS

We obtain the h_c mass, width and branching ratios from simultaneous fits to the π^0 recoil mass distributions for the 16 exclusive η_c decay modes. Here only 1-C kinematic fits with π^0 mass hypothesis are used to improve the energy resolution. The 4C-fits used in event selection are not used in the π^0 recoil mass reconstruction, because the energy resolution of the signal π^0 in 4C-fits is not as good as in the 1C-fits, according to a MC study. From the same data sample we also determine the η_c resonant parameters by fitting the 16 invariant-mass spectra of the hadronic system accompanying the transition photon in $h_c \to \gamma\eta_c$.

A. Fitting the h_c signal

To extract the h_c resonant parameters and the yield for each η_c decay channel, the 16 π^0 recoil mass distributions are fitted simultaneously with a binned maximum likelihood method. A Breit-Wigner function convolved with the instrumental resolution is used to describe the signal shape. An efficiency correction is not needed because of the small h_c width and the good π^0 mass resolution. The resolution function is channel-dependent and is obtained from MC simulation. The parameters $M(h_c)$ and $\Gamma(h_c)$ of the Breit-Wigner function are constrained to be the same for all 16 channels, which is essential for the decay modes with low statistics. For the recoil mass fit to each channel, the background shape is obtained from the η_c mass side bands (2300−2700, 3070−3200 MeV/c^2), and the signal

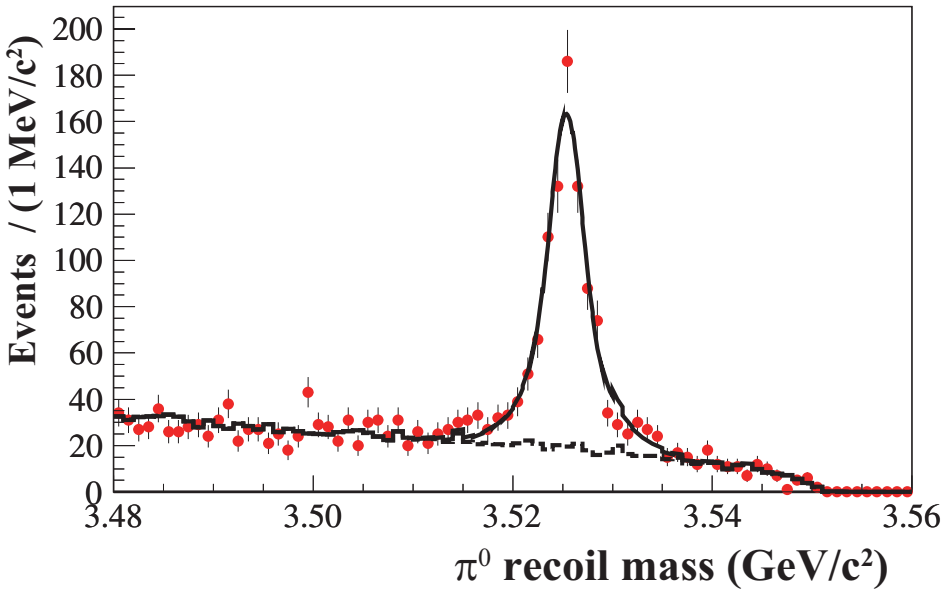

FIG. 1: The π^0 recoil mass spectrum in $\psi(3686) \to \pi^0 h_c, h_c \to \gamma\eta_c$, $\eta_c \to X_i$ summed over the 16 final states X_i. The dots with error bars represent the π^0 recoil mass spectrum in data. The solid line shows the total fit function and the dashed line is the background component of the fit.

and the background normalizations for each mode are allowed to float. The summed and mode-by-mode fit results are shown in Figs. 1 and 2, respectively. The χ^2 per degree of freedom for this fit is 1.60, where sparsely populated bins are combined so that there are at least seven counts per bin in the χ^2 calculation. The parameters of the h_c resonance are determined to be $M(h_c) = 3525.31 \pm 0.11\,\mathrm{MeV}/c^2$ and $\Gamma(h_c) = 0.70 \pm 0.28\,\mathrm{MeV}$, where the errors are statistical only.

The MC-determined selection efficiency ϵ_i and yield N_i for each η_c decay mode are listed in Table II. Based on these numbers, we can calculate the product branching ratios $\mathcal{B}_1(\psi(3686) \to \pi^0 h_c) \times \mathcal{B}_2(h_c \to \gamma\eta_c) \times \mathcal{B}_3(\eta_c \to X_i)$. The branching ratio for $\eta_c \to X_i$ for each of the 16 final states X_i can then be obtained by combining our measurements with $\mathcal{B}_1(\psi(3686) \to \pi^0 h_c) \times \mathcal{B}_2(h_c \to \gamma\eta_c) = (4.36 \pm 0.42) \times 10^{-4}$, the average of two recent measurements by CLEO [9] and BESIII [13]. These branching ratios, with both statistical and systematic errors, are presented in Section VI.

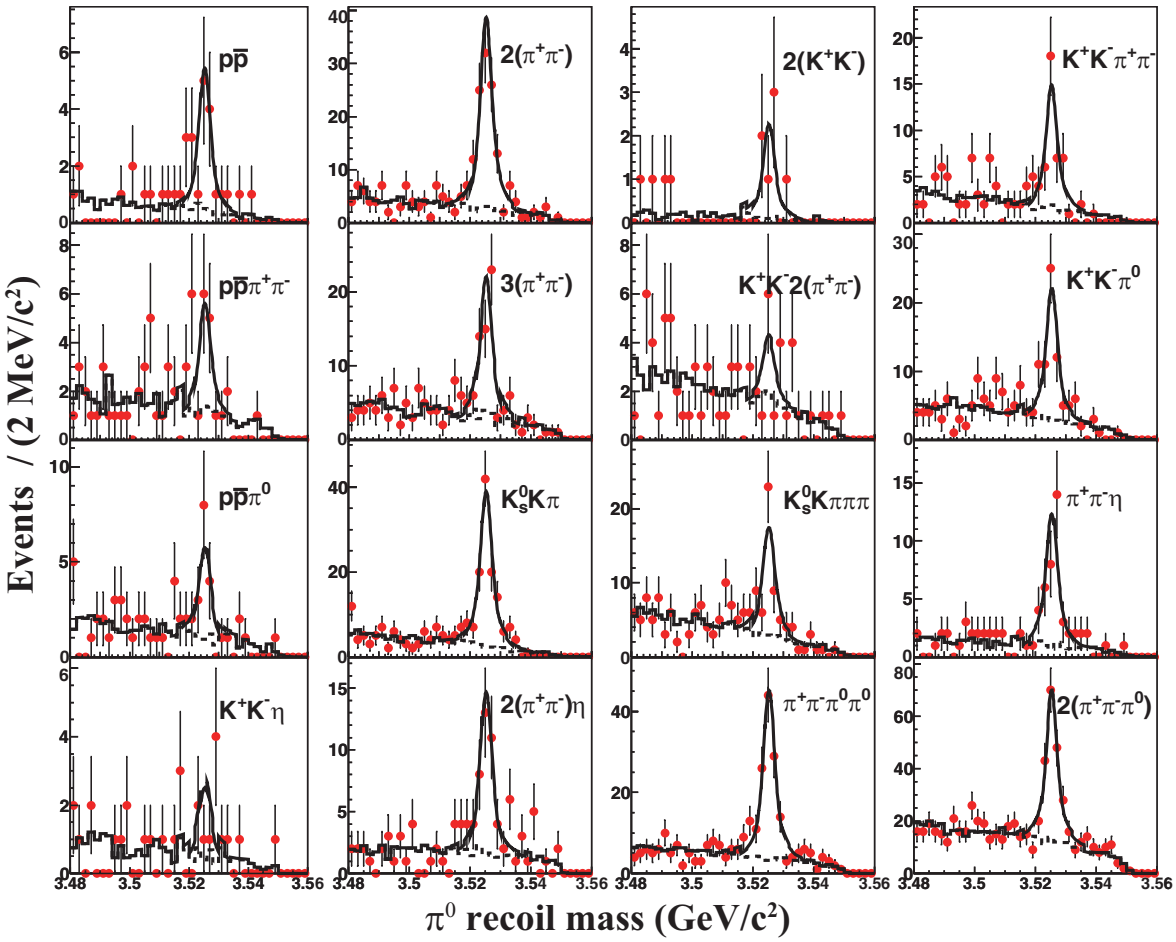

FIG. 2: The simultaneously fitted π^0 recoil mass spectra in $\psi(3686) \to \pi^0 h_c, h_c \to \gamma\eta_c$, $\eta_c \to X_i$ for the 16 final states X_i.

B. Measurement of η_c resonant parameters

In addition to determining the h_c resonant parameters, we can also measure the η_c mass and width with the same event sample. The decay chain $h_c \to \gamma\eta_c$, $\eta_c \to X_i$ is reconstructed and kinematically fitted in the 16 η_c final states X_i. For candidates with satisfactory kinematic fits, we use the resulting track and photon momenta to compute the hadronic mass. We populate distributions of this hadronic mass by removing our previous $E1$ photon-energy and $M(\eta_c)$ requirements and selecting candidates inside a π^0 recoil mass window of $\pm 5\,\mathrm{MeV/c^2}$ around the h_c mass, keeping all other criteria unchanged.

The line shape for the η_c signal for these fits is parameterized as $(E_\gamma^3 \times BW(m) \times f_d(E_\gamma)) \otimes R_i(m)$, where $BW(m)$ is the Breit-Wigner function for η_c as a function of the invariant mass

TABLE II: MC-determined efficiencies ϵ_i and yields N_i for $\psi(3686) \to \pi^0 h_c, h_c \to \gamma\eta_c, \eta_c \to X_i$, where X_i refers to the 16 final states .

Mode	$\epsilon_i(\%)$	N_i
$p\bar{p}$	22.2	15.3 ± 4.5
$\pi^+\pi^-\pi^+\pi^-$	12.6	100.3 ± 11.3
$K^+K^-K^+K^-$	6.6	6.6 ± 2.6
$K^+K^-\pi^+\pi^-$	8.7	38.4 ± 7.0
$p\bar{p}\pi^+\pi^-$	7.8	19.0 ± 5.4
$\pi^+\pi^-\pi^+\pi^-\pi^-\pi^-$	5.4	50.5 ± 9.0
$K^+K^-\pi^+\pi^-\pi^-\pi^-$	2.7	10.3 ± 4.9
$K^+K^-\pi^0$	11.4	54.9 ± 9.2
$p\bar{p}\pi^0$	8.9	14.4 ± 4.6
$K^0_S K^\pm\pi^\mp$	8.9	107.1 ± 11.8
$K^0_S K^\pm\pi^\mp\pi^\pm\pi^\mp$	3.4	43.3 ± 8.0
$\pi^+\pi^-\eta$	4.3	32.9 ± 6.7
$K^+K^-\eta$	3.0	6.7 ± 3.2
$\pi^+\pi^-\pi^+\pi^-\eta$	1.9	38.6 ± 7.6
$\pi^+\pi^-\pi^0\pi^0$	5.5	118.4 ± 12.8
$\pi^+\pi^-\pi^+\pi^-\pi^0\pi^0$	2.2	175.2 ± 17.3
Total	-	831.9±35.0

m of the decay products for each channel, $E_\gamma(m) = \frac{M(h_c)^2 - m^2}{2M(h_c)}$ is the energy of the transition photon in the rest frame of h_c, and $f_d(E_\gamma)$ is a function that damps the divergent tail due to the E_γ^3 factor, which incorporates the energy dependence of the $E1$ matrix element and the phase-space factor. $R_i(m)$ is the signal resolution function for the ith decay mode, which is parameterized by double Gaussians to account for the distorting effects of the kinematic fit and detector smearing. The damping function that we use was introduced by the KEDR collaboration [30]:

$$f_d(E_\gamma) = \frac{E_0^2}{E_\gamma E_0 + (E_\gamma - E_0)^2},$$

where $E_0 = E_\gamma(m_{\eta_c})$ is the $E1$-transition-photon peak energy. The η_c-candidate hadronic invariant mass spectra from low and high side bands in the h_c mass (3500−3515, 3535−3550 MeV/c^2) are used to obtain the background functions for the η_c mass fit. To mitigate the effects of bin-to-bin fluctuations, these side-band mass spectra are smoothed before fitting. A toy MC study was performed to test the effect of the smoothing and it was demonstrated to be a robust procedure that does not systematically distort the fit results. The channel-by-channel signal and background normalizations are free parameters determined by the fit.

We ignore the effect of interference between the signal and background, which was considered in the previous measurement of $\psi(3686) \to \gamma\eta_c$ [20], because the branching ratio of $h_c \to \gamma\eta_c$ is about 50% (branching ratio of $M1$ transition $\psi(3686) \to \gamma\eta_c$ is about 0.3%). The radiative decay of $h_c \to \gamma 0^-$ should be the same level of $\psi(3686) \to \gamma 0^-$, in this case, the non-$\eta_c$ intensity in h_c is much smaller than that for $\psi(3686) \to \gamma\eta_c$.

Figs. 3 and 4 show the hadronic-mass-fit results. The η_c mass and width are determined to be $M(\eta_c) = 2984.49 \pm 1.16\,\mathrm{MeV}/c^2$ and $\Gamma(\eta_c) = 36.4 \pm 3.2\,\mathrm{MeV}$, where the errors are statistical. The χ^2 per degree of freedom for this fit is 1.52, using the same χ^2 calculation method to accommodate low-statistics bins as for the fit to the π^0 recoil mass spectrum.

V. SYSTEMATIC UNCERTAINTIES

A. h_c parameter measurements

The systematic uncertainties for the $M(h_c)$ and $\Gamma(h_c)$ measurements are summarized in Table III. All sources are treated as uncorrelated, so the total systematic uncertainty is obtained by summing them in quadrature. The following subsections describe the procedures and assumptions that led to these estimates of the uncertainties.

1. Energy calibration

The potential inconsistency of the photon-energy measurement between data and MC is evaluated by studying $\psi(3686) \to \gamma\chi_{c1,2}$ ($\chi_{c1,2} \to \gamma J/\psi, J/\psi \to \mu^+\mu^-$) for photons with low energy and radiative Bhabha events for photons with high energy. Discrepancies of 0.4%

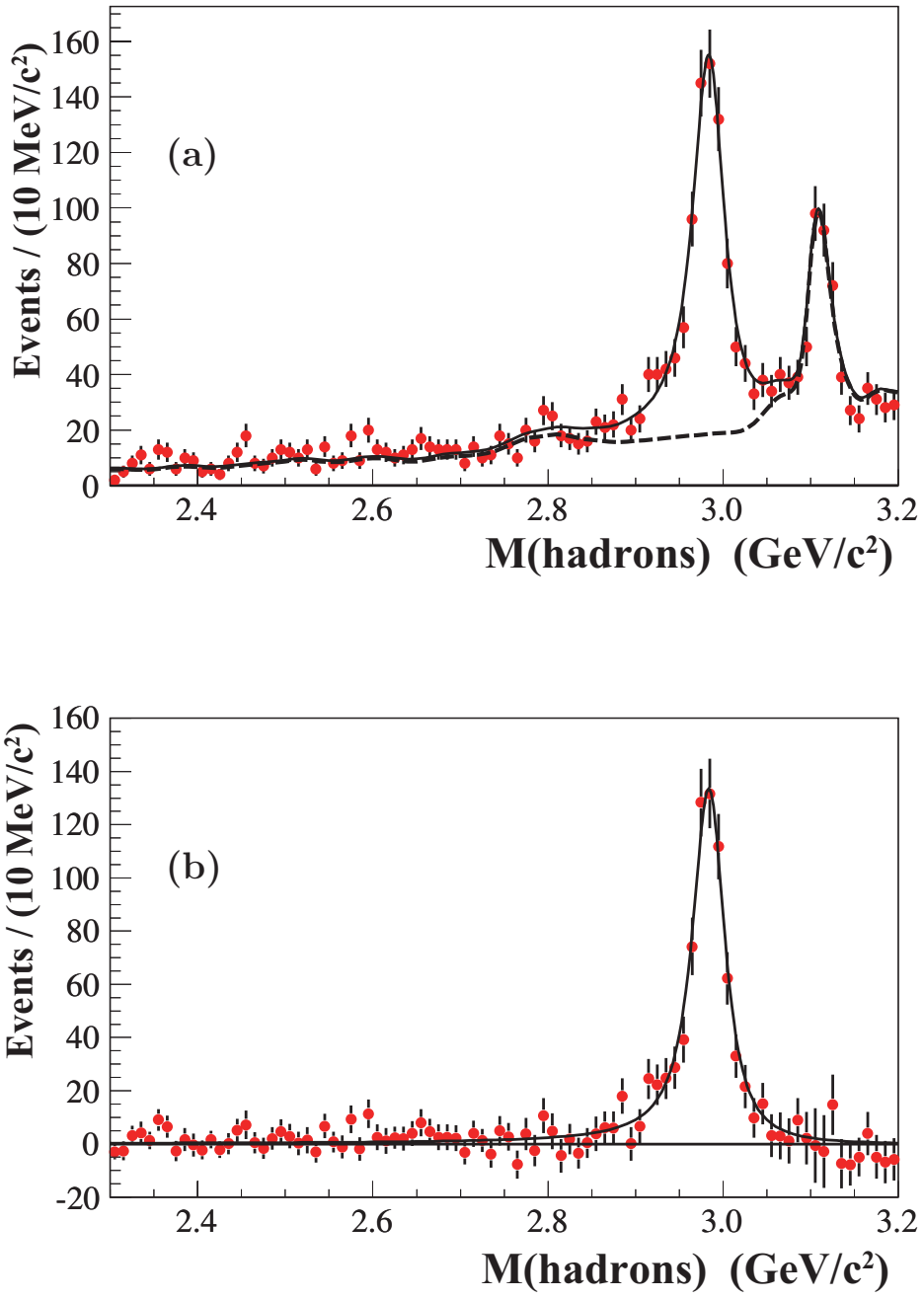

FIG. 3: (a) The hadronic mass spectrum in $\psi(3686) \to \pi^0 h_c, h_c \to \gamma\eta_c$, $\eta_c \to X_i$ summed over the 16 final states X_i. The dots with error bars represent the hadronic mass spectrum in data. The solid line shows the total fit function and the dashed line is the background component of the fit. (b) The background-subtracted hadronic mass spectrum with the signal shape overlaid.

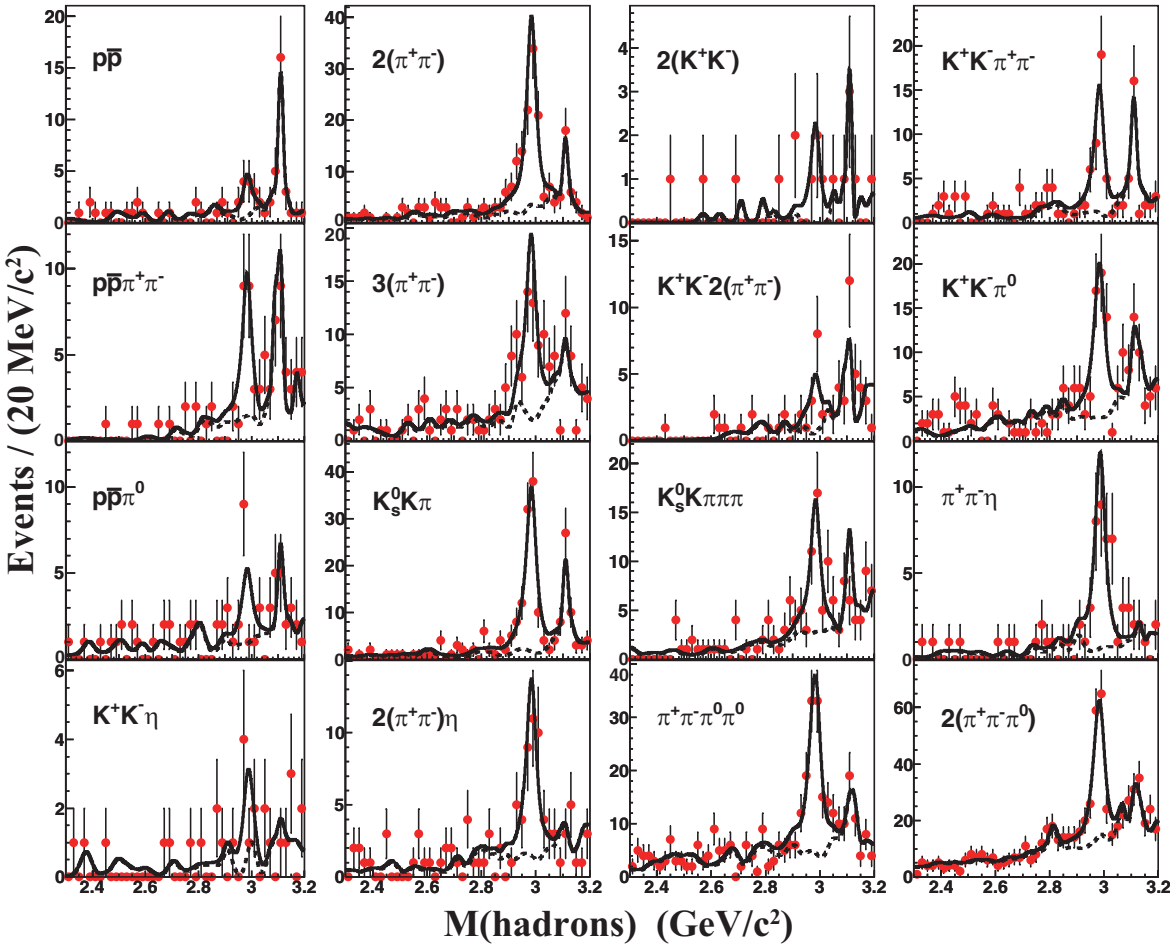

FIG. 4: The simultaneously fitted hadronic mass spectra for the 16 η_c decay channels.

in the energy scale and 4% in the energy resolution between data and MC are found. We vary the photon response accordingly and take the changes in the results as the estimated systematic error. For the $M(h_c)$ measurement, besides the above studies, the reconstructed photon position and error matrix are taken into account as additional sources of uncertainty.

2. Signal shape

The uncertainty associated with the h_c signal shape in the π^0 recoil mass spectrum includes contributions from the photon line shape and the 1-C kinematic fit. We estimate these by determining the changes in results after reasonable adjustments in the photon response. The photon-energy resolution is estimated with the control sample $\psi(3686) \rightarrow$

TABLE III: The systematic errors for the h_c mass and width measurements.

Sources	ΔM_{h_c} (MeV/c^2)	$\Delta\Gamma_{h_c}$ (MeV)
Energy calibration	0.13	0.07
Signal shape	0.00	0.06
Fitting range	0.04	0.16
Binning	0.02	0.01
Background shape	0.01	0.08
Background veto	0.01	0.08
Kinematic fit	0.03	0.03
Mass of $\psi(3686)$	0.03	0.02
Total	0.14	0.22

$\gamma\chi_{c2}$. As above, the energy resolution in data is found to be about 4% worse than in the MC simulation. We correct for this discrepancy by adding single-Gaussian smearing to the energy of the π^0 daughter photons and then using the alternative π^0 shape to redo the fit. The changes in results are assigned as the systematic errors.

3. Fitting range and binning

The systematic uncertainties due to the fitting of the π^0 recoil mass spectrum are evaluated by varying the fitting range and the bin size in the fit. The spreads of results obtained with the alternative assumptions are used to assign the systematic errors.

4. Background shape

To estimate the uncertainty associated with the side-band method for assigning background function shapes, we use an ARGUS function [31] as an alternative background description for each channel and record the changes in the fit results.

5. Background veto

The systematic uncertainties associated with the requirements to suppress background are estimated by varying the excluded ranges.

6. Kinematic fit

Systematic uncertainties caused by the kinematic fit are studied by tuning the tracking parameters and error matrices of charged tracks and photons based on the data. Control samples of $J/\psi \to \phi f_0(980), \phi \to K^+K^-, f_0(980) \to \pi^+\pi^-$, and $\psi(3686) \to \gamma\chi_{cJ}$ are used for this purpose [32]. Channel-by-channel changes of $M(\eta_c)$ and $\Gamma(\eta_c)$ are calculated after the tuning and then averaged by yields and taken as systematic errors.

7. $\psi(3686)$ mass

The systematic uncertainties of the $M(h_c)$ and $\Gamma(h_c)$ determinations associated with the uncertainty in the $\psi(3686)$ mass are estimated to be $0.03\,\mathrm{MeV}/c^2$ and $0.02\,\mathrm{MeV}$, respectively. These are found by shifting $M_{\psi(3686)}$ by one standard deviation according to the PDG value [2] and redetermining the results.

B. η_c branching ratio measurements

The systematic errors in the η_c branching ratio measurements are listed in Tables IV. All sources are treated as uncorrelated, so the total systematic uncertainty is obtained by summing them in quadrature. The following subsections describe the procedures and assumptions that led to the estimates of these uncertainties.

1. Tracking and photon detection

The uncertainty in the tracking efficiency is 2% per track and the uncertainty due to photon detection is 1% per photon [33]. MC studies demonstrate that the trigger efficiency for signal events is almost 100%, so that the associated uncertainty in the results is negligible.

TABLE IV: The systematic errors (in %) in the η_c branching ratio measurements of the η_c exclusive decay channels.

Sources	$p\bar{p}$	$2(\pi^+\pi^-)$	$2(K^+K^-)$	$K^+K^-\pi^+\pi^-$	$p\bar{p}\pi^+\pi^-$	$3(\pi^+\pi^-)$	$K^+K^-2(\pi^+\pi^-)$	$K^+K^-\pi^0$
N($\psi(3686)$)	4.0	4.0	4.0	4.0	4.0	4.0	4.0	4.0
Tracking	4.0	8.0	8.0	8.0	8.0	12.0	12.0	4.0
PID (K_S^0)	2.0	6.0	6.0	4.0	4.0	8.0	8.0	2.0
Photon eff	3.0	3.0	3.0	3.0	3.0	3.0	3.0	5.0
Fit range	2.2	1.2	2.6	2.9	1.5	5.3	3.3	2.7
Bkg shape	10.3	2.5	4.7	0.9	0.3	0.2	3.5	2.8
Signal shape	2.3	2.3	2.3	2.3	2.3	2.3	2.3	2.3
KmFit eff.	7.0	6.3	7.0	8.8	10.8	7.3	4.2	2.0
Bkg veto	5.9	5.5	1.1	0.6	3.1	2.3	5.2	1.7
Cross feed	0.0	2.5	0.0	0.0	0.0	0.0	0.0	1.4
η_c decay models	0.0	2.1	3.7	0.6	2.5	0.0	3.0	4.6
η_c line shape	0.7	0.8	0.6	0.9	0.6	0.6	0.6	0.7
Sum	15.7	14.8	14.9	14.1	15.7	18.0	17.8	10.6

Sources	$p\bar{p}\pi^0$	$K_S^0K^\pm\pi^\mp$	$K_S^0K^\pm\pi^\mp\pi^\pm\pi^\mp$	$\pi^+\pi^-\eta$	$K^+K^-\eta$	$2(\pi^+\pi^-)\eta$	$\pi^+\pi^-\pi^0\pi^0$	$2(\pi^+\pi^-\pi^0)$
N($\psi(3686)$)	4.0	4.0	4.0	4.0	4.0	4.0	4.0	4.0
Tracking	4.0	8.0	12.0	4.0	4.0	8.0	4.0	8.0
PID (K_S^0)	2.0	1.0	1.0	0.0	2.0	0.0	0.0	0.0
Photon eff	5.0	3.0	3.0	5.0	5.0	5.0	7.0	7.0
Fit range	7.7	2.1	1.5	0.6	6.0	1.8	0.6	2.0
Bkg shape	0.1	4.7	4.7	0.1	5.9	0.8	3.3	1.6
Signal shape	2.3	2.3	2.3	2.3	2.3	2.3	2.3	2.3
KmFit eff.	6.8	6.8	7.3	2.0	1.2	6.7	2.4	2.4
Bkg veto	3.7	0.7	2.8	11.8	5.4	14.7	12.8	5.5
Cross feed	0.0	0.0	0.0	0.0	0.0	0.0	1.3	0.0
η_c decay models	5.8	2.5	5.2	5.5	8.1	0.0	0.1	0.5
η_c line shape	0.6	0.6	0.8	0.8	0.7	0.7	0.7	0.7
Sum	14.8	13.2	17.0	15.4	15.3	19.4	16.4	13.3

2. PID and K_S^0 reconstruction

The systematic uncertainties due to kaon and pion identifications are determined to be 2% in Ref. [33]. We choose $J/\psi \to K^{*0}K_S^0, K^{*0} \to K\pi$ to evaluate the efficiency of K_S^0 reconstruction. The 1% difference between data and MC is assigned as the systematic error due to this source.

3. Kinematic fitting

The systematic errors associated with kinematic fitting are estimated by using the control samples of $\psi(3686) \to \pi^0\pi^0 J/\psi$ with J/ψ decay to hadronic final states, which have similar event topology as $\psi(3686) \to \pi^0 h_c, h_c \to \gamma\eta_c$. The average efficiency difference between data and MC, with the same χ^2 requirements in the h_c selection, is taken as the systematic uncertainty.

4. Cross-feed

To evaluate the effect of cross-feed among the 16 signal modes, we use samples of 50,000 MC events per mode. We find that $\eta_c \to 2(\pi^+\pi^-), \eta_c \to K^+K^-\pi^0$ and $\eta_c \to \pi^+\pi^-\pi^0\pi^0$ are contaminated by $\eta_c \to K^0_S K^\pm\pi^\mp$ with levels of 2.5%, 1.4%, and 1.3%, respectively. These numbers are assigned as the systematic errors associated with cross-feed. For other channels, this contamination is found to be negligible.

5. η_c decay models

We use phase space to simulate η_c decays in our analysis. To estimate the systematic uncertainty due to neglecting intermediate states in these decays, we extract invariant masses of η_c daughter particles from $\psi(3686) \to \gamma\eta_c, \eta_c \to X_i$. We analyze MC samples generated according to these invariant masses. To illustrate, Fig. 5 shows the invariant-mass distribution comparison between the data and MC for the decay mode $\eta_c \to K^0_S K^\pm\pi^\mp$. In addition, for channels with low statistics and well-understood intermediate states, MC samples with these intermediate states were generated according to the relative branching ratios given by PDG. The spreads of the efficiencies obtained from the phase-space and alternative MC are taken as the systematic errors.

6. η_c line shape

Because of the η_c mass window requirement in our event selection, the line shape of η_c could be a source of systematic error in the measurement. We vary the input η_c resonant parameters by one standard deviation to estimate the uncertainty due to this source.

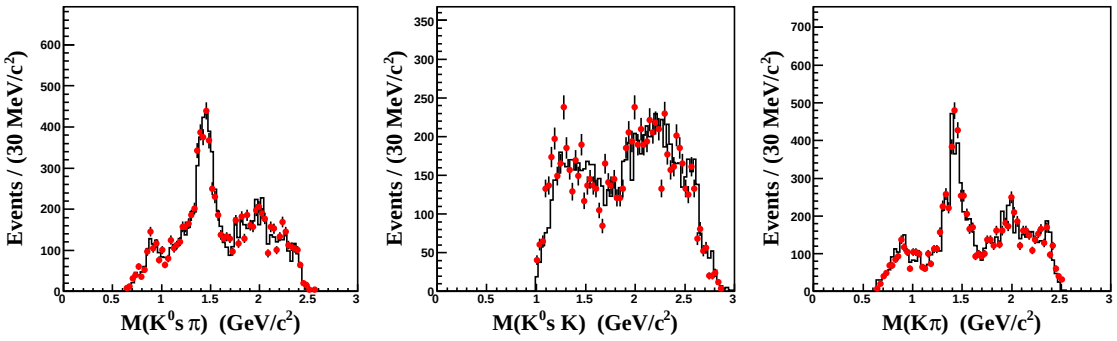

FIG. 5: The dots show the mass spectra for $\psi(3686) \to \gamma\eta_c, \eta_c \to K^0_S K^{\pm}\pi^{\mp}$ in data, and the solid lines are the corresponding mass spectra from the MC simulation.

C. η_c parameter measurements

Systematic errors for the $M(\eta_c)$ and $\Gamma(\eta_c)$ measurements are summarized in Table V. All sources are treated as uncorrelated, so the total systematic uncertainty is obtained by summing in quadrature. The following subsections describe the procedures and assumptions that led to the estimates of these uncertainties.

TABLE V: The systematic errors for η_c parameter measurements.

Sources	M(η_c) (MeV/c^2)	$\Gamma(\eta_c)$ (MeV)
Background shape	0.36	1.45
Fitting range	0.03	0.33
Resolution description	0.10	0.02
Mass-dependent efficiencies	0.11	0.27
Mass-dependent resolutions	0.00	0.01
Kinematic fitting	0.33	0.76
Fitting method	0.11	0.40
Sum	0.52	1.74

1. Background shape

Our standard background shape is the smoothed h_c side-band shape. To estimate the systematic uncertainty due to the background procedure, we change the smoothing level and technique, and vary the h_c side-band ranges. The largest changes in results among these alternatives are assigned as the systematic errors.

2. Fitting range

The systematic uncertainties due to the fitting range are estimated by considering several alternatives to the standard fitting range of 2.3-3.2 $\mathrm{GeV/c^2}$, 2.4-3.2 $\mathrm{GeV/c^2}$, 2.5-3.2 $\mathrm{GeV/c^2}$, 2.6-3.2 $\mathrm{GeV/c^2}$, and 2.3-3.15 $\mathrm{GeV/c^2}$. The systematic uncertainties are assigned to be the largest differences between the standard fit results and those from the alternative ranges.

3. Resolution description

In order to estimate the systematic uncertainties associated with the detector-resolution description, we use MC signal shapes obtained by setting the η_c width to zero as alternatives to double Gaussians. The changes in fit results between these two methods provide the systematic errors.

4. Mass-dependent efficiency and resolution

Since the η_c signal spreads over a sizable mass range, the uncertainties due to the use of mass-independent efficiencies and resolutions need to be estimated. Mass-dependent efficiencies and resolutions are determined from MC simulation and used as an alternative to the default assumption, and the resulting differences are taken to be the systematic errors.

5. Kinematic fitting

The method to evaluate the systematic errors due to the kinematic fitting procedure and momentum measurement is the same as that in the measurement of the h_c parameters.

6. Fitting method

Because we use the smoothed side-band shape to describe the background, the potential for bias due to the smoothing technique must be considered. This was investigated with a toy MC study. We start with a signal sample for each of the 16 channels selected from our standard MC to have the same statistics as data. A corresponding background sample for each channel is constructed from the mass side bands in data. The hadronic-mass distributions for these samples are then treated with a variety of smoothing procedures and fitted. The ranges in the fit results are used to set the systematic errors from this source.

VI. SUMMARY AND DISCUSSION

In summary, we have studied the process $\psi(3686) \to \pi^0 h_c$ followed by $h_c \to \gamma\eta_c$ with an exclusive-reconstruction technique. Using a sample of 106 million $\psi(3686)$ decays we have obtained new measurements of the mass and width of the h_c and η_c charmonium resonances, and of the branching ratios for 16 exclusive η_c hadronic decay modes.

The total yield of events, measured by fitting the π^0 recoil mass spectrum, is 832 ± 35 events, where the error is statistical only. With these events we measure the mass and width of the h_c:

$$M(h_c) = 3525.31 \pm 0.11 \pm 0.14\,\mathrm{MeV/c^2}, \text{ and}$$

$$\Gamma(h_c) = 0.70 \pm 0.28 \pm 0.22\,\mathrm{MeV},$$

where the first errors are statistical and the second are systematic. These results are consistent with the results of a previous inclusive measurement by BESIII [13]:

$$M(h_c) = 3525.40 \pm 0.13 \pm 0.18\,\mathrm{MeV/c^2}, \text{ and}$$

$$\Gamma(h_c) < 1.44\,\mathrm{MeV} \text{ (at 90\% confidence level)}.$$

The branching-ratio results $\mathcal{B}_1(\psi(3686) \to \pi^0 h_c) \times \mathcal{B}_2(h_c \to \gamma\eta_c) \times \mathcal{B}_3(\eta_c \to X_i)$ and $\mathcal{B}_3(\eta_c \to X_i)$ are given in Table VI, quoted with the statistical and systematic errors of this measurement and, for $\mathcal{B}_3$, an additional systematic error associated with the input branching-ratio product $\mathcal{B}_1(\psi(3686) \to \pi^0 h_c) \times \mathcal{B}_2(h_c \to \gamma\eta_c)$. Most of our $\mathcal{B}_3(\eta_c \to X_i)$

TABLE VI: $\mathcal{B}_1(\psi(3686) \to \pi^0 h_c) \times \mathcal{B}_2(h_c \to \gamma\eta_c) \times \mathcal{B}_3(\eta_c \to X_i)$ and $\mathcal{B}_3(\eta_c \to X_i)$ with systematic errors. The third errors in $\mathcal{B}_3$ measurement are systematic errors due to uncertainty of $\mathcal{B}_1(\psi(3686) \to \pi^0 h_c) \times \mathcal{B}_2(h_c \to \gamma\eta_c)$.

X_i	$\mathcal{B}_1 \times \mathcal{B}_2 \times \mathcal{B}_3$ ($\times 10^{-6}$)	$\mathcal{B}_3$ (%)	$\mathcal{B}_3$ in PDG (%)
$p\bar{p}$	0.65 ± 0.19 ± 0.10	0.15±0.04±0.02±0.01	0.141±0.017
$\pi^+\pi^-\pi^+\pi^-$	7.51 ± 0.85 ± 1.11	1.72±0.19±0.25±0.17	0.86±0.13
$K^+K^-K^+K^-$	0.94 ± 0.37 ± 0.14	0.22±0.08±0.03±0.02	0.134±0.032
$K^+K^-\pi^+\pi^-$	4.16 ± 0.76 ± 0.59	0.95±0.17±0.13±0.09	0.61±0.12
$p\bar{p}\pi^+\pi^-$	2.30 ± 0.65 ± 0.36	0.53±0.15±0.08±0.05	<1.2 (at 90% C.L.)
$\pi^+\pi^-\pi^+\pi^-\pi^+\pi^-$	8.82 ± 1.57 ± 1.59	2.02±0.36±0.36±0.19	1.5±0.50
$K^+K^-\pi^+\pi^-\pi^-\pi^-$	3.60 ± 1.71 ± 0.64	0.83±0.39±0.15±0.08	0.71±0.29
$K^+K^-\pi^0$	4.54 ± 0.76 ± 0.48	1.04±0.17±0.11±0.10	1.2±0.1
$p\bar{p}\pi^0$	1.53 ± 0.49 ± 0.23	0.35±0.11±0.05±0.03	–
$K^0_S K^\pm\pi^\mp$	11.35 ± 1.25 ± 1.50	2.60±0.29±0.34±0.25	2.4±0.2
$K^0_S K^\pm\pi^\mp\pi^\pm\pi^\mp$	12.01 ± 2.22 ± 2.04	2.75±0.51±0.47±0.27	–
$\pi^+\pi^-\eta$	7.22 ± 1.47 ± 1.11	1.66±0.34±0.26±0.16	4.9±1.8
$K^+K^-\eta$	2.11 ± 1.01 ± 0.32	0.48±0.23±0.07±0.05	<1.5 (at 90% C.L.)
$\pi^+\pi^-\pi^+\pi^-\eta$	19.17 ± 3.77 ± 3.72	4.40±0.86±0.85±0.42	–
$\pi^+\pi^-\pi^0\pi^0$	20.31 ± 2.20 ± 3.33	4.66±0.50±0.76±0.45	–
$\pi^+\pi^-\pi^+\pi^-\pi^0\pi^0$	75.13 ± 7.42 ± 9.99	17.23±1.70±2.29±1.66	–

branching-fraction results are consistent with PDG values [2], and several branching fractions are measured for the first time.

Combining our measurement of $M(h_c)$ with the previously-determined mass of the centroid of the ^3P_J states leads to

$$\Delta\ M_{hf} \equiv \langle M(1^3P)\rangle - M(1^1P_1) = -0.01 \pm 0.11\ (\text{stat.}) \pm 0.15\ (\text{syst.})\,\text{MeV/c}^2, \qquad (1)$$

consistent with the lowest-order expectation that the $1P$ hyperfine splitting is zero.

The line shape of η_c was also studied from the $E1$ transition $h_c \to \gamma\eta_c$, and the measured resonant parameters are:

$$M(\eta_c) = 2984.49 \pm 1.16 \pm 0.52\,\text{MeV/c}^2, \text{and}$$

$$\Gamma(\eta_c) = 36.4 \pm 3.2 \pm 1.7\,\text{MeV}.$$

These results are consistent with the recent BESIII results from $\psi(3686) \to \gamma\eta_c$ [20]:

$$M(\eta_c) = 2984.3 \pm 0.6 \pm 0.6\,\text{MeV/c}^2, \text{and}$$

$$\Gamma(\eta_c) = 32.0 \pm 1.2 \pm 1.0\,\mathrm{MeV};$$

and B-factory results from $\gamma\gamma \to \eta_c$ and B decays [17, 18]. Because of the larger $\psi(3686)$ data sample that will be coming from BESIII and the advantage of negligible interference effects, we expect that $h_c \to \gamma\eta_c$ will provide the most reliable determinations of the η_c resonant parameters in the future.

VII. ACKNOWLEDGMENTS

The BESIII collaboration thanks the staff of BEPCII and the computing center for their hard efforts. This work is supported in part by the Ministry of Science and Technology of China under Contract No. 2009CB825200; National Natural Science Foundation of China (NSFC) under Contracts Nos. 10745001, 10625524, 10821063, 10825524, 10835001, 10935007, 11125525; Joint Funds of the National Natural Science Foundation of China under Contracts Nos. 11079008, 11179007, 10979058; the Chinese Academy of Sciences (CAS) Large-Scale Scientific Facility Program; CAS under Contracts Nos. KJCX2-YW-N29, KJCX2-YW-N45; 100 Talents Program of CAS; Istituto Nazionale di Fisica Nucleare, Italy; Ministry of Development of Turkey under Contract No. DPT2006K-120470; U. S. Department of Energy under Contract Nos. DE-FG02-04ER41291, DE-FG02-91ER40682, DE-FG02-94ER40823; U.S. National Science Foundation; University of Groningen (RuG); the Helmholtzzentrum fuer Schwerionenforschung GmbH (GSI), Darmstadt; and WCU Program of National Research Foundation of Korea under Contract No. R32-2008-000-10155-0.

---

[1] E. Eichten, K. Gottfried, T. Kinoshita, K. D. Lane and T. -M. Yan, Phys. Rev. D **17**, 3090 (1978) [Erratum-ibid. D **21**, 313 (1980)].

[2] J. Beringer *et al.* [Particle Data Group], Phys. Rev. D**86**, 010001 (2012).

[3] S. K. Choi *et al.* [BELLE Collaboration], Phys. Rev. Lett. **89**, 102001 (2002) [Erratum-ibid. **89**, 129901 (2002)]; K. Abe *et al.* [BELLE Collaboration], Phys. Rev. Lett. **98**, 082001 (2007).

[4] D. M. Asner *et al.* [CLEO Collaboration], Phys. Rev. Lett. **92**, 142001 (2004).

[5] B. Aubert *et al.* [BABAR Collaboration], Phys. Rev. D **72**, 031101 (2005).

[6] M. Ablikim *et al.* [BESIII Collaboration], Phys. Rev. Lett. **109**, 042003 (2012).

[7] See, for example, E. S. Swanson, Phys. Rep. **429**, 243 (2006), and references therein.

[8] M. Andreotti *et al.* [E835 Collaboration], Phys. Rev. D **72**, 032001 (2005).

[9] S. Dobbs *et al.* [CLEO Collaboration], Phys. Rev. Lett. **101**, 182003 (2008).

[10] T. A. Armstrong *et al.* [E760 Collaboration], Phys. Rev. Lett. **69**, 2337 (1992).

[11] J. L. Rosner *et al.* [CLEO Collaboration], Phys. Rev. Lett. **95**, 102003 (2005).

[12] G. S. Adams *et al.* [CLEO Collaboration], Phys. Rev. D **80**, 051106 (2009).

[13] M. Ablikim *et al.* [BESIII Collaboration], Phys. Rev. Lett. **104**, 132002 (2010).

[14] J. Y. Ge *et al.* [CLEO Collaboration], Phys. Rev. D **84**, 032008 (2011).

[15] T. K. Pedlar *et al.* [CLEO Collaboration], Phys. Rev. Lett. **107**, 041803 (2011).

[16] T. Himel *et al.*, Phys. Rev. Lett. **45**, 1146 (1980).

[17] A. Vinokurova *et al.* [Belle Collaboration], Phys. Lett. B **706**, 139 (2011).

[18] P. del Amo Sanchez *et al.* [BABAR Collaboration], Phys. Rev. D **84**, 012004 (2011).

[19] R. E. Mitchell *et al.* [CLEO Collaboration], Phys. Rev. Lett. **102**, 011801 (2009) [Erratum-ibid. **106**, 159903 (2011)].

[20] M. Ablikim *et al.* [BESIII Collaboration], Phys. Rev. Lett. **108**, 222002 (2012).

[21] M. Ablikim *et al.* [BESIII Collaboration], Nucl. Instrum. Meth. A **614**, 345 (2010).

[22] M. Ablikim *et al.* [BESIII Collaboration], Phys. Rev. D **81**, 052005 (2010).

[23] S. Agostinelli *et al.* [GEANT4 Collaboration], Nucl. Instrum. Meth. A **506**, 250 (2003); Geant4 version: v09-03p0; Physics List simulation engine: BERT; Physics List engine packaging library: PACK 5.5.

[24] J. Allison *et al.*, IEEE Trans. Nucl. Sci. **53**, 270 (2006).

[25] R. G. Ping, Chinese Physics C **32**, 8 (2008).

[26] S. Jadach , B. F. L. Ward and Z. Was, Comp. Phys. Commun. **130**, 260 (2000); S. Jadach, B. F. L. Ward and Z. Was, Phys. Rev. D **63**, 113009 (2001).

[27] D.J. Lange, Nucl. Instrum. Meth. A **462**, 152 (2001).

[28] T. Sjostrand, Comput. Phys. Commun. **82**, 74 (1994).

[29] M. Xu, *et. al.*, Chinese Physics C **33**, 428 (2009).

[30] V.V. Anashin *et al.*, arXiv:1012.1694 [hep-ex].

[31] H. Albrecht *et al.* [ARGUS Collaboration], Phys. Lett. B **241**, 278 (1990).

[32] M. Ablikim *et al.* [BESIII Collaboration], arXiv:1208.4805 [hep-ex].

[33] M. Ablikim *et al.* [BESIII Collaboration], Phys. Rev. D **83**, 112005 (2011).